

Towards a Unified Textual Graph Framework for Spectral Reasoning via Physical and Chemical Information Fusion

Jiheng Liang^b, Ziru Yu^{a,*}, Zujie Xie^b, Yuchen Guo^c, Yulan Guo^a and Xiangyang Yu^b

^aSchool of electronics and communication engineering, Sun Yat-Sen University, Shenzhen, 518107, China

^bSchool of Physics, State Key Laboratory of Optoelectronic Materials and Technologies, Sun Yat-Sen University, Guangzhou, 510275, China

^cGuangzhou Guangxin Technology Co., LTD, Guangzhou, 510300, China

ARTICLE INFO

Keywords:

Textual Graphs
Multi-modal Language Models
Graph Neural Network
Chemical functional groups
Spectral Analysis

ABSTRACT

Motivated by the limitations of current spectral analysis methods—such as reliance on single-modality data, limited generalizability, and poor interpretability—we propose a novel multi-modal spectral analysis framework that integrates prior knowledge graphs with Large Language Models. Our method explicitly bridges physical spectral measurements and chemical structural semantics by representing them in a unified Textual Graph format, enabling flexible, interpretable, and generalizable spectral understanding. Raw spectra are first transformed into TAGs, where nodes and edges are enriched with textual attributes describing both spectral properties and chemical context. These are then merged with relevant prior knowledge—including functional groups and molecular graphs—to form a Task Graph that incorporates "Prompt Nodes" supporting LLM-based contextual reasoning. A Graph Neural Network further processes this structure to complete downstream tasks. This unified design enables seamless multi-modal integration and automated feature decoding with minimal manual annotation. Our framework achieves consistently high performance across multiple spectral analysis tasks, including node-level, edge-level, and graph-level classification. It demonstrates robust generalization in both zero-shot and few-shot settings, highlighting its effectiveness in learning from limited data and supporting in-context reasoning. This work establishes a scalable and interpretable foundation for LLM-driven spectral analysis, unifying physical and chemical modalities for scientific applications.

1. Introduction

Spectral analysis serves as a fundamental tool in numerous scientific and industrial domains, including material science, chemical analysis, biomedical diagnostics, food safety, and environmental monitoring [1, 2, 3, 4]. It involves techniques such as near-infrared (NIR), mid-infrared (MIR), Raman, and ultraviolet-visible (UV-Vis) spectroscopy, each providing valuable insights into molecular vibrations, electronic transitions, and absorption characteristics at microscopic scales [5]. However, interpreting spectral data in isolation frequently yields ambiguous results due to overlapping spectral features, limited dataset sizes, and insufficient contextual information [5]. To achieve accurate and meaningful interpretations, spectral data often necessitate integration with auxiliary knowledge, such as chemical structures, textual scientific annotations, or domain-specific expertise.

Multi-modal analysis, which integrates data from diverse modalities such as images, text, graphs, and structured domain knowledge, has emerged as a powerful methodology to overcome the inherent limitations of single-modality data analysis [6, 7]. By leveraging complementary features across

modalities, multi-modal techniques offer enhanced analytical capabilities, improved interpretability, and superior generalization performance [8]. Prior studies have primarily applied multi-modal spectral analysis to the classification and analysis of complex materials, utilizing combinations of Fourier Transform Infrared (FTIR), Raman, and Laser-induced Breakdown Spectroscopy (LIBS) data [9]. Concurrently, graph-based approaches have gained attention due to their ability to explicitly model relationships between spectral features and relevant chemical or biomedical properties, further enhancing predictive accuracy and interpretability [10].

Recently, Large Language Models (LLMs), including GPT-4, PaLM, and BERT, have demonstrated exceptional capabilities in multi-modal reasoning, generalization, and adaptability, significantly advancing fields beyond traditional natural language processing (NLP) [11, 12, 13, 14]. These models exhibit remarkable proficiency in understanding and generating human-like text, processing diverse data modalities, and extracting complex patterns from extensive datasets [15, 16]. Trained on vast corpora encompassing a wide spectrum of textual and contextual information, LLMs are particularly adept at encoding semantic relationships, reasoning over structured data, and generating coherent, interpretable insights [17]. Consequently, integrating LLMs with spectral analysis holds considerable promise, offering the ability to efficiently contextualize spectral information with external domain knowledge. Such integration enhances interpretability, generalizability, and adaptability of spectral analyses, making LLMs highly suitable for addressing the

*Corresponding author. School of electronics and communication engineering, Sun Yat-Sen University, Shenzhen, 518107, China

✉ liangjh65@mail2.sysu.edu.cn (J. Liang); yuziru@mail.sysu.edu.cn (Z. Yu); xiezj8@mail2.sysu.edu.cn (Z. Xie); guoyuchen@guangxin.tech (Y. Guo); guoyulan@sysu.edu.cn (Y. Guo); cesyxy@mail2.sysu.edu.cn (X. Yu)

ORCID(s): 0009-0004-5522-0884 (J. Liang); 0000-0002-9763-8806 (Z. Yu); 0009-0000-1945-1045 (Z. Xie); 0000-0001-7051-841X (Y. Guo); 0000-0001-6673-3221 (X. Yu)

inherent complexities and challenges in multi-modal spectral frameworks.

1.1. Related Work

1.1.1. Multi-modal Representation

A pivotal aspect of multi-modal learning is the development of effective representation techniques that can seamlessly combine information from various modalities. Deep learning approaches have been instrumental in this regard[18], offering robust frameworks for capturing intricate relationships between different data types. For instance, Guo et al.[19] provided a comprehensive survey on deep multimodal representation learning, highlighting its capacity to model complex interactions across modalities.

Traditionally, researchers have designed complex structures to train data and obtain unified representations. These approaches typically follow two main paths: feature fusion and attention mechanisms. In 2019, Zhou et al.[20] proposed a unique method for learning latent representations, which can handle multi-modal data, such as MRI, PET, and genetic information. Their approach involves designing a complex integrated framework that combines dimensionality reduction, classification, and feature fusion. On the other hand, Mao et al.[21] introduced a novel approach using an attention-based multi-modal framework to generate a joint speech and text representation. While these studies demonstrate the potential of creating effective representations through complex multi-modal and multi-step workflows, a significant shortcoming of these methods is their poor generalizability. Specifically, representations trained using such complex frameworks often struggle to adapt to unseen data or tasks. Moreover, these encoding methods may not transfer effectively across different applications.

With the rise of powerful language models, researchers have turned to using semantic encoding from pre-trained language models as unified representations. For instance, Agbavor et al.[22] leveraged the deep representation features of Data2Vec and Wav2Vec2-classical semantic embeddings introduced in 2019-and refined an end-to-end model with fully connected layers to enhance Alzheimer's disease detection. More recently, Zhou et al.[23] explored the benefits of pre-training BERT on a cancer-specific dataset to extract breast cancer phenotypes from pathology reports and clinical records. Their findings emphasized the importance of domain-specific pre-training, which substantially improved model performance by making it more attuned to the nuances of domain-specialized data.

1.1.2. Knowledge Graph

Traditional knowledge graphs (KGs) have predominantly been constructed using single-modal data, and such single-modal KGs have proven to be highly effective in several research areas. For instance, in medical diagnostics, single-modal KGs that focus on structured clinical data have been successfully employed to assist in clinical decision-making. A key example is the work by Li et al.[24], which utilized a clinical knowledge graph to enhance diagnostic

accuracy in cancer patients by integrating patient records, treatment regimens, and disease pathways.

However, despite the success of single-modal KGs, their limitations have become increasingly apparent, particularly when attempting to capture the full spectrum of information necessary for more comprehensive spectral analysis. Spectral data is inherently multi-dimensional and involves various types-ranging from time-series spectra and hyperspectral images to spectral signatures from different sources and environmental conditions, which are decided by complex and multiple physical factors. Limiting knowledge graphs to a single modality neglects crucial relationships and interactions between these diverse data types, thereby impeding their ability to represent the complexity of real-world spectral scenarios.

As a result, the need for multi-modal knowledge graphs (MMKGs) has gained increasing attention, as they can combine and integrate multiple data sources to produce richer, more complete representations of medical knowledge. An example is the work by Wang et al.[25]. This evolving trend indicates the necessity to further develop multi-modal knowledge graphs that can better represent the complexity and diversity of data in modern spectral analysis. Moreover, there has been increasing research aimed at improving the interpretability of AI models by leveraging prior knowledge in knowledge graphs. In the context of near-infrared (NIR) spectroscopy, a novel interpretable ensemble learning method has been developed to enhance the rapid characterization of petroleum products[26]. This approach improves trust in AI systems by allowing professionals to understand and validate the reasoning behind the AI's decisions.

1.1.3. Generalization of Downstream Tasks

In recent years, there has been growing recognition of the importance of generalizing AI models to perform effectively across a variety of downstream tasks and scenarios, particularly those closely connected to real-world applications. For example, in the field of biomedicine, where tasks often require models to adapt to dynamic and diverse data sources, Tu et al.[27] have developed generalist biomedical AI systems capable of interpreting multiple data modalities, such as clinical language, imaging, and genomics, within a unified framework.

The predominant approach for achieving generalization has been transfer learning, which involves fine-tuning pre-trained models on specific downstream tasks. Transfer learning has been widely adopted due to its efficiency and effectiveness in reducing the need for extensive task-specific data. In spectral research, a novel multi-stage active transfer learning framework[28] has been proposed for near-infrared, integrating a domain shift method and using in the pharmaceutical, chemical, and food industries.

Despite its successes, transfer learning has inherent limitations. It often requires substantial task-specific data for fine-tuning, which can be scarce in specialized domains. Additionally, the imbalance data would also be block for utilizing transfer learning, while it is a common situation

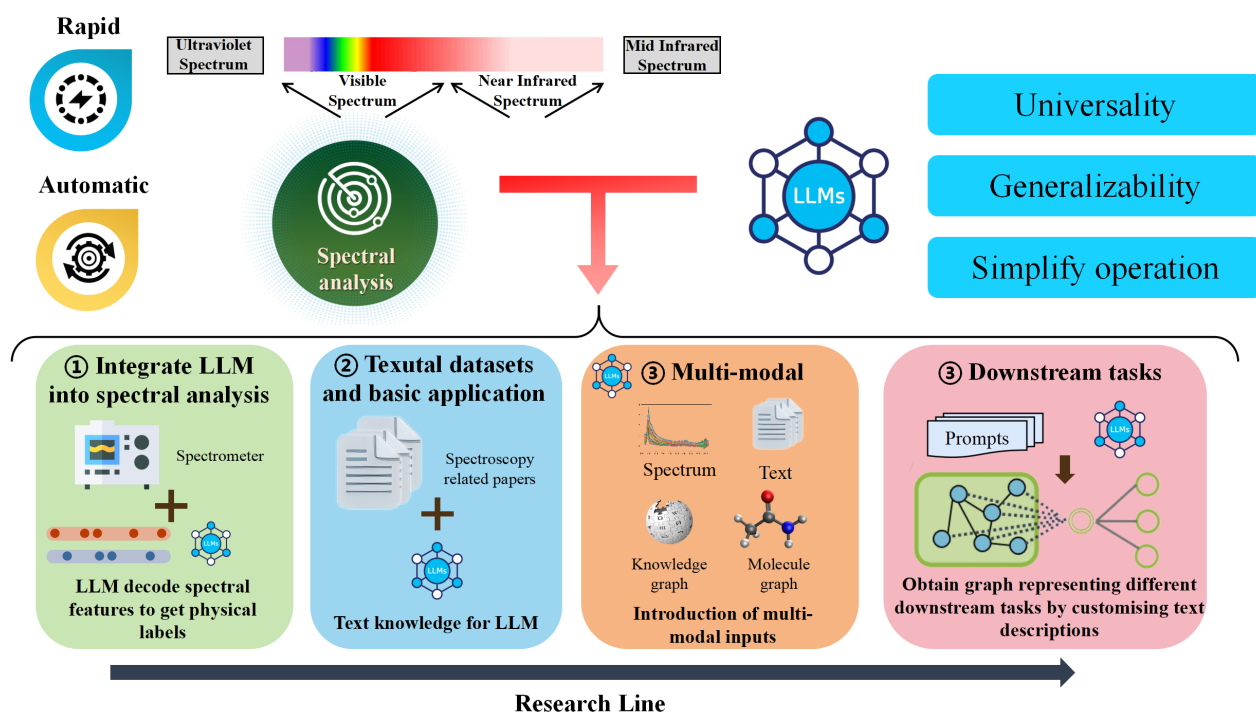


Figure 1: The figure illustrates the overall research motivation and direction of integrating large language models (LLMs) into spectral analysis. Traditional spectral analysis spans from ultraviolet to mid-infrared regions and aims for rapid and automatic interpretation of spectral data. By embedding LLMs, the workflow evolves through four stages: (1) integrating LLMs with spectrometers to decode spectral features into physical labels, (2) leveraging spectroscopy-related textual data to enhance LLM understanding, (3) introducing multi-modal inputs such as text, knowledge graphs, and molecular structures, and (4) customizing prompt-based downstream task representations through graph construction. This integration improves universality, generalizability, and operational simplicity in spectral applications.

in real-world application. On the other hand, the fine-tuned model may overfit to the target task, reducing its ability to generalize further. These drawbacks limit the scalability and adaptability of transfer learning, particularly in rapidly evolving fields.

With the advent of LLMs like ChatGPT, there is a new opportunity to leverage their inherent generalizability in our models. ChatGPT, as explored in Zhou et al.[29], demonstrates remarkable flexibility across a wide range of tasks without extensive retraining, owing to its ability to generalize knowledge from pre-training. By incorporating this LLMs' component into our own models, we aim to enhance the adaptability to reduce the dependency on task-specific fine-tuning while expanding their applicability to diverse real-world scenarios. This method also aligns the unified representation we select before.

1.2. Our contribution

Despite recent advancements, multi-modal spectral analyses still face significant limitations. Current approaches primarily focus on integrating multiple spectral modalities or limited structured data, neglecting broader chemical textual knowledge and comprehensive knowledge graphs [30]. Additionally, existing methodologies often lack scalability, limiting their applicability in diverse real-world contexts.

Overcoming these limitations necessitates novel strategies that effectively combine spectral data with textual and structured domain knowledge to support more generalized and accurate spectral interpretations.

Multi-modal data are ubiquitous across various domains, offering enhanced information richness and robustness, especially in scenarios with incomplete or corrupted data. Yet, mainstream spectral analysis techniques predominantly focus on single-modality data, underutilizing the extensive prior knowledge accumulated from previous studies. To bridge this gap, our initial objective is to establish a unified representation framework for multi-modal data, integrating text and graph, and raw spectra commonly used in spectral analysis.

We further envision deploying this unified spectral processing framework in practical scenarios with limited computational resources, typical of industrial environments where full-scale LLMs may not be economically feasible. Consequently, we propose leveraging LLM-based embedding encoders to map diverse data types into a shared semantic space, requiring the conversion of different modalities into structured textual representations. Such representations facilitate effective integration of spectral data with prior knowledge sources.

Motivated by these insights, we introduce a novel multi-modal spectral analysis framework that combines spectral data, textual scientific literature, and structured domain knowledge (e.g., molecular and knowledge graphs) using LLMs. By integrating physical measurements from spectra with chemically grounded knowledge representations, our approach enables a unified understanding of spectral patterns rooted in both physical signal characteristics and chemical semantics. It capitalizes on the multi-modal reasoning capabilities of LLMs to automate complex feature decoding, significantly reducing manual annotation efforts and extending spectral analysis applicability across scientific fields.

Specifically, our proposed framework addresses existing limitations by directly utilizing raw spectral inputs and incorporating multi-modal prior knowledge to improve interpretability and generalizability. The core innovation involves transforming query spectra into a TAG representation, where nodes and edges store textual attributes. This TAG representation unifies spectral data with additional modalities, including chemical structures and functional group information, enabling seamless integration and embedding processing by LLMs. Subsequently, we construct a Merging Graph by linking the query TAG with relevant multi-modal knowledge, forming a Task Graph. The Task Graph includes prompt nodes that anchor contextual information and guide analysis toward customized downstream tasks such as functional group prediction. Finally, a GNN processes the entire graph structure to generate the desired analytical outputs.

The proposed framework specifically comprises four essential components:

- We introduce a framework that fuses spectral data, functional group textual descriptions, and structured chemical knowledge via textual graphs, enabling chemically meaningful reasoning and improved interpretability.
- By integrating LLMs, the system supports diverse input forms and natural language interaction, enhancing generalizability, reducing annotation effort, and simplifying usage.
- LLM-driven prompt learning enables flexible, task-specific spectral interpretation, supporting multiple downstream tasks (judgment, classification, generation, analysis).
- The Textual Graph design ensures seamless multimodal integration and provides a scalable foundation for extending the framework to various spectral analysis scenarios.

2. Preliminary

2.1. Textual Graph

A textual graph is a structured graph representation in which both nodes and edges are associated with natural language descriptions as attributes. Formally, a textual graph is defined as:

$$\mathcal{G} = (\mathcal{V}, \mathcal{E}, \mathcal{A}) \quad (1)$$

where $\mathcal{V} = \{v_1, v_2, \dots, v_{|\mathcal{V}|}\}$ is the set of nodes, and $\mathcal{E} \subseteq \mathcal{V} \times \mathcal{V}$ is the set of directed edges.

The attribute set $\mathcal{A} = \{\mathcal{A}_{\mathcal{V}}, \mathcal{A}_{\mathcal{E}}\}$ includes textual information attached to nodes and edges. Each node $v \in \mathcal{V}$ is associated with a textual description \mathcal{A} , and each directed edge $(v_i, v_j) \in \mathcal{E}$ is associated with a relation label a and its textual description $\mathcal{A}_{\mathcal{E}}$, forming a relation triple:

$$e_{ij} = (v_i, a, v_j) \quad (2)$$

The adjacency structure of the graph is represented by a binary matrix $\mathbf{M} \in \{0, 1\}^{|\mathcal{V}| \times |\mathcal{V}|}$, indicating node connectivity.

2.2. Textual Graph Transformation

In general, based on transformation methods designed using domain-specific expertise, most types of data can be converted into TAG. Given an arbitrary data type, a sample $\mathbf{X} \in \mathbb{R}^{\mathcal{N}}$ can be extracted. There exists a transformation function T that generates a set of subsets $\mathbf{x}_i \in \mathbb{R}^{N_i}$, each capturing essential information from the original data, as shown in Equation (3):

$$\{\mathbf{x}_i\}_{i=1}^N = T(\mathbf{X}), T : \mathbb{R}^{\mathcal{N}} \rightarrow \bigcup_{i=1}^N \mathbb{R}^{N_i}. \quad (3)$$

$\mathbb{R}^{\mathcal{N}}$ is original data space and N_i is split sub-space. Generally, we have $\bigcup_{i=1}^N \mathbb{R}^{N_i} \subseteq \mathbb{R}^{\mathcal{N}}$. The transformation T may take different forms across various research tasks, depending on specific application requirements. Common operations include entity extraction, dimensionality reduction, and conditional filtering. Subsequently, another transformation S is applied to generate metadata from the derived subsets, where each metadata instance consists of a feature and its corresponding identifier. This facilitates the differentiation and recognition of relevant information in each \mathbf{x}_i , as illustrated in Equation (4):

$$\{(\mathbf{z}_i, \text{name}_i)\}_{i=1}^N = S(\{\mathbf{x}_i\}_{i=1}^N), \quad \mathbf{x}_i \in \mathbb{R}^{N_i}, \quad (4)$$

$$S : \bigcup_{i=1}^N \mathbb{R}^{N_i} \rightarrow \bigcup_{i=1}^N (\mathbf{z}_i \times N). \quad (5)$$

In the metadata, \mathbf{z}_i and name_i represent the extracted feature from \mathbf{x}_i and its corresponding identifier, respectively. The metadata set $\mathbf{z}_i, \text{name}_i$ adopts a task-specific structure. For example, if \mathbf{x}_i corresponds to a characteristic absorption peak in a spectral signal, the transformation S extracts metadata such as the peak value and full width at half maximum in scalar form. Alternatively, if \mathbf{x}_i refers to a tag extracted from a scientific article, the resulting metadata will include textual information and its associated label name. Based on such standardized metadata, the nodes, edges, and attributes of the text graph can be constructed, as illustrated in Equation (6):

$$\mathcal{G} = \begin{cases} \mathcal{V}_i = \{\text{Node}(\mathbf{z}_i) \mid \mathbf{z}_i \in \{\mathbf{z}_i\}^{\text{node}}\}, \\ \mathcal{E}_i = \{\text{Edge}(\mathbf{z}_i) \mid \mathbf{z}_i \in \{\mathbf{z}_i\}^{\text{edge}}\}, \\ \mathcal{A}_{\mathcal{V}_i} = \{\text{LLM}(\mathbf{z}_i, \text{name}_i) \mid \mathbf{z}_i \in \{\mathbf{z}_i\}^{\text{node}}\}, \\ \mathcal{A}_{\mathcal{E}_i} = \{\text{LLM}(\mathbf{z}_i, \text{name}_i) \mid \mathbf{z}_i \in \{\mathbf{z}_i\}^{\text{edge}}\}. \end{cases} \quad (6)$$

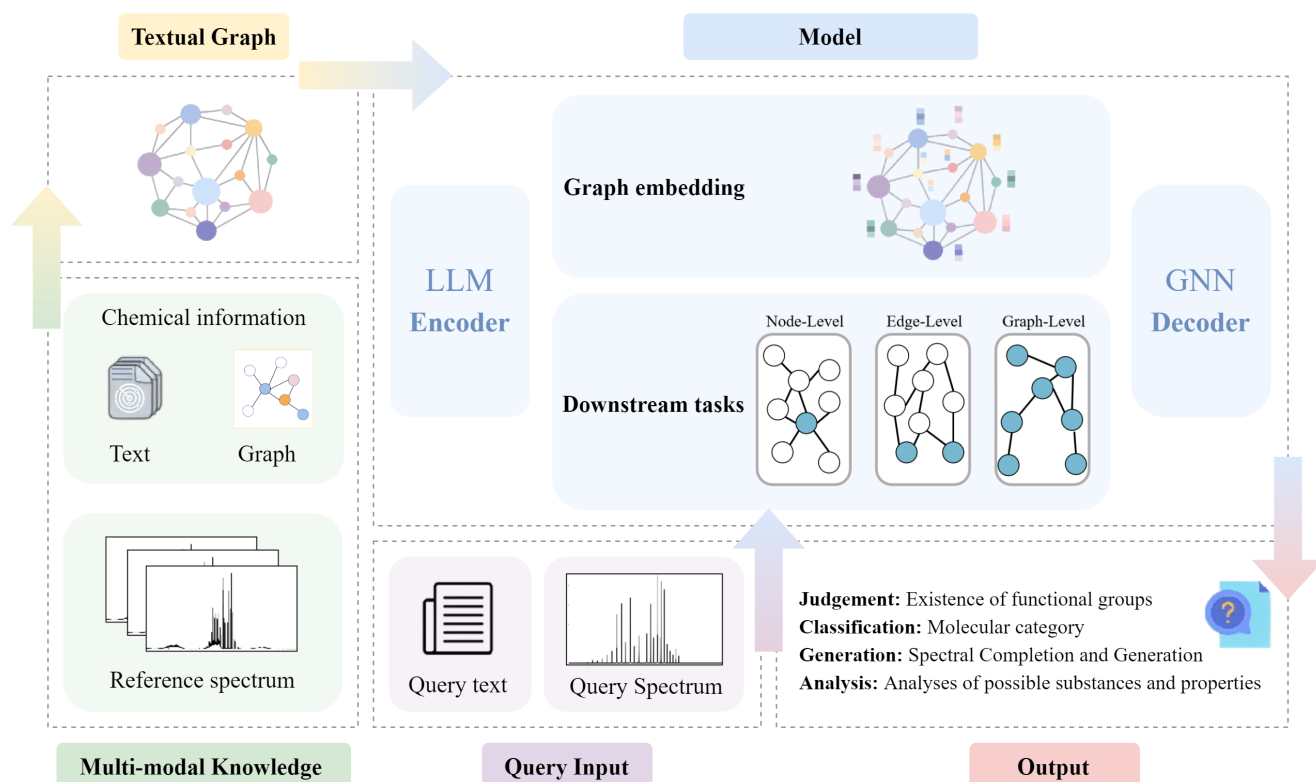


Figure 2: The workflow begins by converting spectral data into a TAG representation, while multi-modal prior knowledge—such as molecular structures and chemical ontologies—is similarly transformed into TAG format. These two components are then linked to establish semantic connections between spectral features and domain knowledge. Finally, task-specific subgraphs are introduced, and the entire graph is processed through LLM-based encoding and decoding to produce the corresponding task outputs.

The functions Node() and Edge() are used to generate nodes and edges, respectively. With the assistance of any LLMs, textual features can be derived from \mathbf{z}_i and $name_i$, and stored as node and edge attributes, denoted by $\mathcal{A}_{\mathcal{V}_i}$ and $\mathcal{A}_{\mathcal{E}_i}$. In addition, \mathbf{z}_i^{node} and \mathbf{z}_i^{edge} are subsets of the full set $\{\mathbf{z}_i, name_i\}_{i=1}^N$, used specifically for constructing nodes and edges, respectively. The partitioning is determined by identifier tokens embedded in $name_i$ through the transformation S , as shown in Equation (7):

$$\begin{aligned} \{\mathbf{z}_i\}^{node} &= \{\mathbf{z}_i \mid \{(z_i, name_i)\}_{i=1}^N, name_i \text{ contains 'node'}\}, \\ \{\mathbf{z}_i\}^{edge} &= \{\mathbf{z}_i \mid \{(z_i, name_i)\}_{i=1}^N, name_i \text{ contains 'edge'}\}. \end{aligned} \quad (7)$$

Additionally, it is worth noting that after the transformation S , the pair $(\mathbf{z}_i, name_i)$ could, in principle, be directly encoded, allowing scalar, vector, or textual \mathbf{z}_i values to be transformed into semantic embeddings via the LLMs. However, we intentionally avoid this approach because LLMs typically do not treat numerical values as atomic units. Instead, they tend to tokenize and encode numbers into subword segments, which may compromise the integrity of numeric information. Such fragmentation may negatively affect both the prediction accuracy and robustness of the proposed spectral information processing framework in downstream tasks.

To mitigate this, we organize each $(\mathbf{z}_i, name_i)$ pair into a complete natural language sentence before encoding, as illustrated in Equation (6). Although LLMs may still split

the numeric values during tokenization, the added contextual information helps preserve the semantic integrity of the numerical data. This approach is also more aligned with natural human expression. For example, mentioning a feature name and value separately in conversation often lacks clarity, while a full descriptive statement is more likely to ensure the two pieces of information are perceived as semantically linked.

3. Unified Textual Graph Processing Framework

We propose the spectral information processing framework illustrated in Figure 2. This framework adopts the TAG \mathcal{G} as a unified representation of multimodal data, encodes all textual content into a shared semantic space using LLMs, and introduces task-specific subgraph structures to support various downstream spectral analysis tasks.

3.1. Merging Graph

To integrate spectral signals with chemical knowledge, we construct a merging graph by fusing an infrared or near-infrared spectrum $\mathbf{X} \in \mathbb{R}^{\mathbb{N}}$ with a structured chemical knowledge graph. This enables cross-modal reasoning between spectral patterns and molecular functional groups, as illustrated in Figure 3.

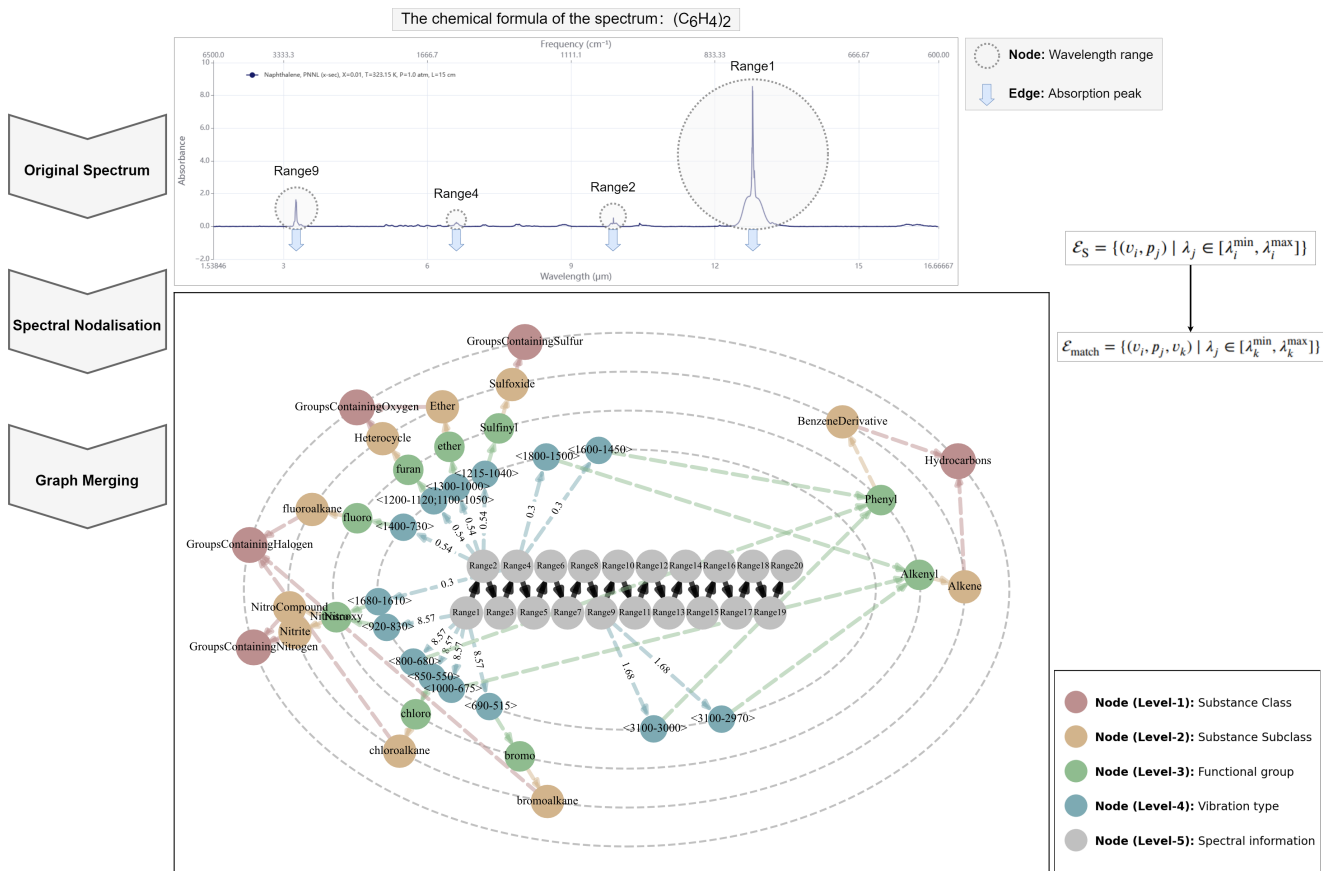


Figure 3: (a) Continuous spectral data are discretized into multiple "Range" nodes. For intervals containing absorption peaks, additional edges are added to indicate peak presence. (b) The resulting spectral graph is integrated with the chemical knowledge graph to form a merged graph. Each "Range" nodes(gray) is linked via edges(blue) to corresponding "Vibration Type" nodes(blue) in the knowledge graph, with hierarchical connections to higher-level nodes also shown.

The input spectrum \mathbf{X} is first converted into TAG representation $\mathcal{G}_S = (\mathcal{V}_S, \mathcal{E}_S, \mathcal{A}_S)$, which captures the structured properties of spectral data. The construction process includes the following components:

- **Node Construction:** The full spectral range is evenly divided into N intervals, with each node v_i representing a wavelength range:

$$\mathcal{V}_S = \{v_i = [\lambda_i^{\min}, \lambda_i^{\max}]\}, \quad (8)$$

where $[\lambda_i^{\min}, \lambda_i^{\max}]$ denotes the i -th wavelength interval.

- **Edge Construction:** For each absorption peak p_j , an edge is created between its corresponding spectral range node v_i :

$$\mathcal{E}_S = \{(v_i, p_j) \mid \lambda_j \in [\lambda_i^{\min}, \lambda_i^{\max}]\}. \quad (9)$$

The absorption intensity of each peak is incorporated as the edge weight, reflecting its spectral significance.

To enrich this spectral graph with chemical semantics, we define a structured chemical knowledge graph $\mathcal{G}_K =$

$(\mathcal{V}_K, \mathcal{E}_K, \mathcal{A}_K)$, which includes hierarchical relationships between vibration types and substance class, as described in detail in Section 4.2.2.

To bridge the spectral and chemical modalities, we establish a cross-modal mapping that links spectral range nodes to vibration-type nodes. The resulting matching edges retain the hierarchical structure of the chemical graph while introducing weighted links that quantify the correlation between spectral peaks and vibration types based on absorption intensity.

Specifically, for each spectral range node v_i containing an absorption peak p_j , we identify all vibration-type nodes v_k whose characteristic frequency range $[\lambda_k^{\min}, \lambda_k^{\max}]$ contains the peak wavelength λ_j . The resulting set of matching edges is defined as:

$$\mathcal{E}_{\text{match}} = \{(v_i, p_j, v_k) \mid \lambda_j \in [\lambda_k^{\min}, \lambda_k^{\max}]\}. \quad (10)$$

To reduce false-positive associations and enhance the reliability of the fused graph, we implement a refinement mechanism based on negative correlation filtering. For each functional group f , we first identify its characteristic vibration region, which corresponds to a set of spectral segment nodes.

The confidence score τ_f for functional group f is computed as the ratio of spectral segments within $\mathcal{V}_f \subset \mathcal{V}_K$ that are connected to absorption peaks:

$$\tau_f = \frac{1}{|\mathcal{V}_f|} \sum_{v_k \in \mathcal{V}_f} \mathbb{1}(v_k \in \mathcal{E}_{match}) \quad (11)$$

Here, $\mathbb{1}(\cdot)$ denotes the indicator function, which returns 1 if the vibration-type node of functional group v_k is connected to an spectral node v_i (i.e., an absorption peak) via an edge in \mathcal{E}_{match} , and 0 otherwise. The resulting score $\tau_f \in [0, 1]$ quantifies the proportion of characteristic wavelength nodes associated with functional group f that exhibit spectral activity.

Functional groups with scores below a predefined threshold τ are considered weakly supported and are pruned from the knowledge graph:

$$\mathcal{E}_{match} \leftarrow \mathcal{E}_{match} \setminus \{v_f \in \mathcal{V}_f \mid \tau_f < \tau\} \quad (12)$$

Finally, to ensure the structural compactness and task relevance of the fused graph, we apply a series of graph optimization strategies. A subgraph extraction operation centered on spectral nodes is performed, where a hop-based constraint maintains local connectivity while eliminating redundant or weakly relevant links. Additionally, the sample node is connected to all relevant spectral segment nodes, enabling instance-level reasoning and downstream prediction tasks.

3.2. Task Graph

In Equation (6), the node set \mathcal{V} and edge set \mathcal{E} associate with attributes recorded in the attribute set \mathcal{A} . At this stage, the unstructured data has been fully transformed into a unified TAG representation. In practice, researchers can follow the above procedure and design customized data transformation pipelines according to the specific requirements of their domain. Subsequently, a different LLMs from the one used for generating attributes to construct \mathcal{A} and a LLaMA-based model for encoding will be employed to encode the textual information in the graph. This step embeds the node and edge attributes, originally expressed in natural language, into high-dimensional vectors, thereby mapping all textual information into a unified semantic space:

$$\mathcal{G}_{encoder} = \text{LLM}(\mathcal{G}). \quad (13)$$

Here, $\mathcal{H}_{encoder}$ correspond to the vector representations of graph. All embeddings are one-dimensional vectors whose lengths depend on the specific LLMs used for text encoding. At this stage, we have successfully executed a standardized conversion from the general data type to the TAG format.

Typically, different training or inference strategies must be designed for each task level, making it difficult to unify them within a single framework. However, given the strong generalization capability of LLMs to adapt to various downstream tasks via natural language prompts, our LLMs-based

spectral information processing framework offers the flexibility to support multiple task types within a unified structure. To this end, we design a task sub-graph that complements the merging graph, collectively forming the complete task graph \mathcal{G}_{task} . This design enables seamless switching between node-level, edge-level, and graph-level tasks via prompt semantics, without changing the overall graph topology.

To execute inference over this unified structure, the complete task graph \mathcal{G}_{task} is passed through a graph neural network to compute high-level semantic representations for all relevant nodes. This decoding process is formulated as:

$$\mathcal{H}_{decoder} = \text{GNN}(\mathcal{G}_{task}). \quad (14)$$

Here, $\mathcal{H}_{decoder}$ denotes the output feature matrix containing hidden representations of all nodes in the task graph after multiple GNN layers. These representations are used by the downstream classifier to generate final predictions for node-level, edge-level, or graph-level tasks, depending on how the prompt and response nodes are connected within \mathcal{G}_{task} .

Once the complete task graph structure \mathcal{G}_{task} is constructed, LLMs-based embedding is used to map all textual content within \mathcal{G}_{task} into a unified semantic space. In addition to incorporating the prior knowledge and generalization capabilities of LLMs, this approach eliminates the need to learn graph representations from scratch—a process that typically requires large and high-quality training datasets. After embedding, a GNN is employed to process the entire graph and produce analytical results. The GNN aggregates and propagates relevant information within \mathcal{G}_{task} , and after multiple network layers, the "Response Node" output the final classification results of the framework. This method offers the advantage of significantly fewer parameters compared to full-scale LLMs, enabling faster computation and lower resource consumption, making it a more practical choice for real-world applications.

In this framework, the task sub-graph comprises two key components: the prompt node and the response node, both of which are decoded using the same text embedding mechanism as in the merging graph.

3.2.1. Prompt Node

Downstream tasks on graph-structured data can be categorized into three levels: node-level, edge-level, and graph-level. The specific objectives for tasks at each level are as follows: Node task involves inferring the category or label of a specific node within the graph; Edge task focuses on determining the type of relationship between any two nodes; Graph task aims to assign an entire graph instance to a predefined category based on the information from all its nodes and edges.

Each prompt node v_p encodes a specific downstream task through textual attributes that include background context, task description, and output expectations. It connects to the

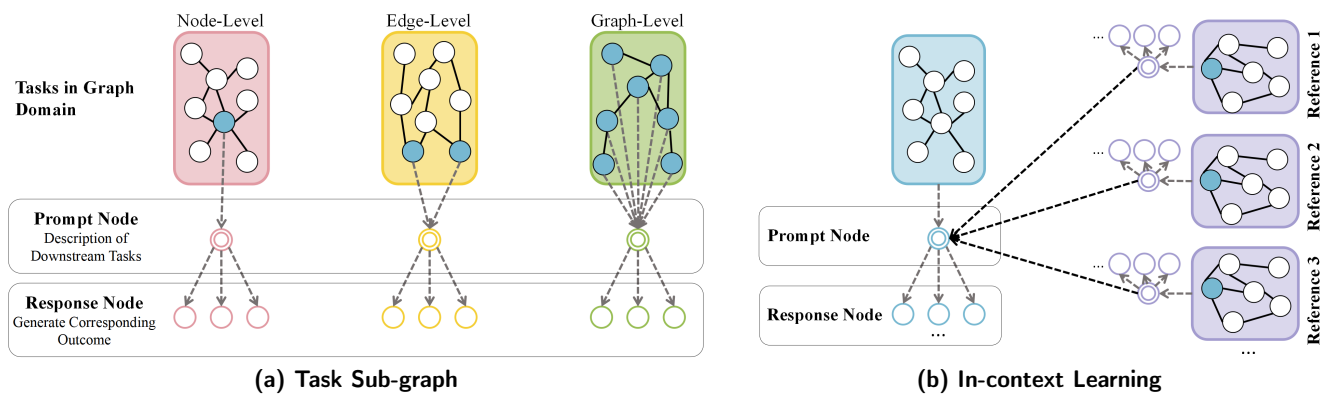


Figure 4: (a) This structure introduces customized downstream tasks and integrates different levels of graph tasks into a unified framework through connection strategies with the merging graph. (b) In the zero-shot setting, no reference examples are connected; in the few-shot setting, a specified number of reference examples are introduced.

merging graph \mathcal{G} based on the granularity of the task:

$$\begin{aligned} \text{Node-level: } & (v_p, v_t) \in \mathcal{E}_{task}, \\ \text{Edge-level: } & (v_p, v_{t_1}), (v_p, v_{t_2}) \in \mathcal{E}_{task}, \\ \text{Graph-level: } & (v_p, v_t) \in \mathcal{E}_{task}, \forall v_t \in \mathcal{V}_t, \end{aligned} \quad (15)$$

where $\mathcal{V}_t \subseteq \mathcal{V}$ denotes the subset of task-relevant nodes v_t selected from the merging graph, and \mathcal{E}_{task} represents the set of task-specific edges used to link v_p to these nodes. This connection strategy allows all tasks to be defined uniformly, with only the prompt node's connectivity varying by task level.

3.2.2. Response Node

Response nodes are introduced to capture the outputs of downstream tasks in a unified manner. Depending on the task type, a response node v_r may correspond to a class label, a binary decision, a continuous spectrum output, or a natural language explanation. After passing the task graph \mathcal{G}_{Task} through a multi-layer GNN [31], the final representation \mathbf{h}_{v_r} of the response node is obtained via an attention-based layer aggregation mechanism. Specifically, we compute:

$$\mathbf{h}_{v_r} = H \cdot \text{Softmax} \left((\mathbf{W}_K H)^\top \cdot \mathbf{W}_Q \mathbf{h}_{v_r}^{(0)} \right) \quad (16)$$

where $H = [\mathbf{h}_{v_r}^{(1)}, \dots, \mathbf{h}_{v_r}^{(L)}] \in \mathbb{R}^{d \times L}$ denotes the matrix composed of hidden states from L GCN layers for node v_r . Each column $\mathbf{h}_{v_r}^{(l)}$ is the representation of node v_r after the l -th GCN layer. Here, d is the dimensionality of the node feature vectors, which also serves as the projection space for attention computation.

The initial node representation is set as $\mathbf{h}_{v_r}^{(0)} = \mathbf{h}_{A_v}$, corresponding to the LLM-encoded vector based on the node's textual name and attribute. The matrices $\mathbf{W}_K \in \mathbb{R}^{d_K \times d}$ and $\mathbf{W}_Q \in \mathbb{R}^{d_Q \times d}$ are learnable linear projections used to compute the key and query representations, respectively. In practice, we set $d_K = d_Q = d'$ to unify the attention space.

This attention-based decoding mechanism enables the model to adaptively assign importance weights to intermediate representations across different GCN layers, depending

on the specific reasoning requirement of the downstream task. By fusing multi-layer signals in a task-adaptive way, the response node representation \mathbf{h}_{v_r} becomes more expressive and robust.

Based on the type of downstream task, the final output of the response node \mathbf{h}_{v_r} is interpreted differently:

(1) *Judgment Task.* For the edge-level classification task, the framework aims to infer latent relationships between different absorption peaks within the spectrum. For instance, given two nodes with edges from the query spectrum, the framework must predict whether both peaks originate from the same functional group. The prompt node connects to both of these nodes with edges, and the task is framed as a binary classification problem.

At the graph level, the framework predicts the chemical category of the molecule corresponding to the entire query spectrum. For example, given a query spectrum, the framework determines whether the corresponding molecule is an aromatic compound. This type of task is referred to as "graph judgement" and is also framed as a binary classification task, where the prompt node is connected to all nodes in the merging graph.

Additionally, we introduce another binary graph-level classification task, distinct from graph judgment by using specific functional groups as labels with explicit semantic meaning. This task, referred to as graph classification, is designed to assess the effectiveness of semantic encoding within the framework. All molecules used in the experiments are carefully selected to ensure structural simplicity, allowing the framework to make reasonably accurate predictions based on infrared spectral data.

For binary decision tasks (e.g., peak-pair similarity, graph-level judgment), a sigmoid function is applied:

$$\hat{Y} = \text{Sigmoid}(\mathbf{h}_{v_r}) \quad (17)$$

We use a binary cross-entropy (BCE) loss:

$$\mathcal{L}_{Jdg} = - [Y \log \hat{Y} + (1 - Y) \log(1 - \hat{Y})] \quad (18)$$

This formulation supports binary labels $Y \in \{0, 1\}$ and yields probabilistic confidence for decision tasks.

(2) *Classification Task*. In the subsequent experiments, we design spectral classification tasks at different levels. For the node-level classification task, the framework is required to identify the category of functional group corresponding to a specific absorption peak in the query spectrum. For example, given a spectral node connected to an absorption peak edge in the query spectrum and a set of candidate functional groups, the framework must determine which group is most likely responsible for the observed vibrational absorption. In this case, the prompt node is connected to the target spectral node with edge, and the task is formulated as a multi-class classification problem.

For tasks with c possible categories (e.g., functional group identification), the model outputs a probability distribution:

$$\hat{Y} = \text{Softmax}(\mathbf{h}_{v_r}), \quad c \in \{1, \dots, C\} \quad (19)$$

We apply a cross-entropy loss:

$$\mathcal{L}_{cls} = - \sum_{c=1}^C Y \log(\hat{Y}) \quad (20)$$

where Y is the one-hot encoded ground truth label.

(3) *Generation Task*. For generation tasks, the framework predicts a synthetic spectrum based on the semantic representation of a molecular query. The corresponding atomic position and atomic number vectors are retrieved from a knowledge base. Given a natural language input, a fine-tuned LLM extracts the molecular formula, which is encoded and propagated through the task graph to produce a response node embedding \mathbf{h}_{v_r} .

The response nodes are then fed into CNN [32], to simulate the molecule's spectrum. This architecture effectively captures spatial dependencies to generate high-fidelity spectral data. In this case, the generation module is implemented via a learned convolutional network. The final spectrum output is computed as:

$$\hat{Y} = \text{CNN}(\mathbf{h}_{v_r}) \quad (21)$$

This output $\hat{Y} \in \mathbb{R}^\lambda$ corresponds to the predicted spectrum over λ wavelength positions.

For continuous spectrum generation tasks, the predicted spectrum \hat{Y} is trained using mean squared error (MSE) against the ground truth spectrum Y :

$$\mathcal{L}_{gen} = \frac{1}{\lambda} \sum_{i=1}^{\lambda} \|\hat{Y}_i - Y_i\|_2 \quad (22)$$

This loss encourages the generated spectral signal to preserve peak positions, intensities, and shapes.

(4) *Analysis Task*. In analysis tasks, the framework is expected to generate a free-form textual response based on spectral information and embedded domain knowledge. Given a query prompt, the Response Node v_r produces a hidden representation \mathbf{h}_{v_r} , which is then decoded into a natural language answer:

$$\hat{Y} = \text{LLM}(\mathbf{h}_{v_r}) \quad (23)$$

Here, \hat{Y} denotes a generated sentence or paragraph (e.g., "The absorption peak at 1720 cm^{-1} corresponds to C=O stretching in ketones.").

To train this module, we apply a standard token-level cross-entropy loss between the generated text and the reference text Y , assuming an autoregressive generation framework:

$$\mathcal{L}_{ana} = - \sum_{t=1}^T \log P(Y_t | Y_{<t}) \quad (24)$$

where T is the length of the target text sequence and Y_t is the t -th token in the ground truth explanation.

This task enables the framework to deliver interpretable, human-readable outputs, and facilitates human-AI interaction in scientific reasoning scenarios such as functional group interpretation, classification rationale explanation, or spectral anomaly description.

4. Multi-modal Data

4.1. Physical Spectral Data

In spectral analysis, informative content is typically concentrated around a few absorption peaks, making full-spectrum processing unnecessary. By focusing on these peaks, we reduce dimensionality while preserving predictive performance. Our framework discretizes continuous spectra into nodes and edges based on absorption peaks, achieving near-perfect AUC scores in edge classification and graph-level prediction tasks.

Following the base transformation to extract absorption peaks and convert them into discrete "Range" nodes (Figure 3). Each peak is bounded along the wave number axis and mapped to a node. A total of n such nodes are created, with the remaining spectral regions uniformly divided into 20 fixed "Range Nodes."

We then apply \mathcal{S} to generate node metadata. For peak-containing nodes, metadata include intensity, standard intensity, full width at half maximum, and interval length; others retain only the interval length. Each spectral segment \mathbf{z}_i is converted to a textual description s via LLM and appended to the node. If a peak is present, an additional "Absorption Peak" edge is created to store all metadata except the interval range.

4.2. Chemical information

In spectral analysis, identifying functional groups behind absorption peaks relies heavily on prior knowledge. Beyond spectral libraries, scientific literature and knowledge graphs

also offer valuable insights. However, multi-modal knowledge integration remains underexplored. To bridge this gap, we adopt textual attribute graphs to unify diverse data types-text, spectral images, and chemical knowledge graphs-for downstream tasks like molecular spectrum classification.

4.2.1. Textual Data

We use the SDAAP dataset[33], a structured literature corpus on spectral analysis. The research subjects within the SDAAP textual database and the spectral image repository are primarily macroscopic samples-such as meat, fruits, vegetables, and medicinal herbs-which provide limited useful information for spectral analysis at the molecular level, particularly when focusing on functional group-based interpretation.

Each document is transformed into a TAG via transformation T , extracting labels and their names. Then, S constructs a graph with a central "Paper" node linked to multiple "Label" nodes (Figure 5). Documents are organized under "Research Domain" nodes for thematic clustering, with orange sub-nodes further detailing each domain.

In practice, when a spectrum is queried, relevant prior knowledge is retrieved by linking spectral nodes to literature nodes. If over 50% of a query peak's range overlaps with a document's "Reference Spectrum" node, a connection is established to transfer contextual spectral knowledge.

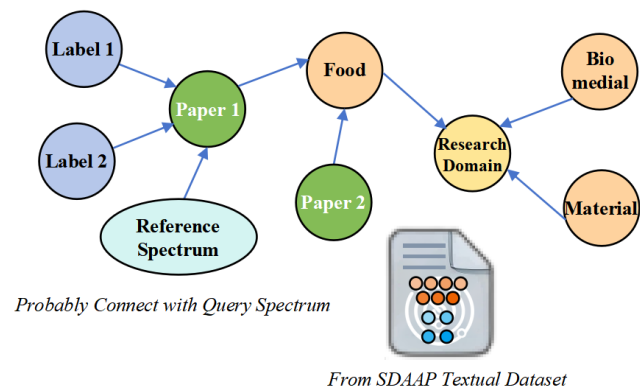


Figure 5: TAG Representation of Textual Data. Literature entries from the SDAAP dataset are node-structured based on their associated labels and subsequently aggregated according to their respective research domains.

When a query spectrum is input in real-world applications, prior knowledge from the literature database can be incorporated by connecting spectral nodes to potentially related document nodes. In most manuscripts, authors typically provide reference spectra of the studied samples, from which relevant absorption peak information can be extracted and stored in cyan "Reference Spectrum" node as part of the document labels. A connection is established between a query absorption peak and a literature absorption peak node when their absorption range overlap exceeds 50%.

4.2.2. Chemistry Knowledge Graph

Knowledge graphs structure complex relationships among entities, enabling efficient information retrieval. In chemical analysis, they are widely used to link compounds with elements, diseases, and drugs [34, 35]. For spectral analysis, functional group information is particularly crucial, as it directly influences spectral absorption features.

Many existing chemical knowledge graphs are structurally mature and require only minor preprocessing for integration. Building on the comprehensive graph by Fang et al. [36], which includes elements, functional groups, and chemical properties, we further incorporate vibrational modes and absorption data to construct a spectral-relevant knowledge base.

The node information for all compounds is extracted from the chemical functional group knowledge graph and text information, including:

- **Substance Class:** Used to trace the relationship between the major substance classes and their subclasses, helping to distinguish different substance categories such as organic and inorganic compounds.
- **Substance Subclass:** Used to track the subclasses of substances within a major category, further classifying different types of compounds, such as alcohols, acids, etc.
- **Functional Group:** The core node of the knowledge graph, containing the name, chemical representation, and related information of functional groups, representing the chemical functional characteristics of substances.
- **Vibration Type:** Describes the substructure, vibration type, and vibration intensity of functional groups, storing the characteristic wavelength ranges associated with functional groups, which may include multiple wavelength intervals, helping to characterize molecular vibration properties.

As shown in Figure 6, the graph is organized hierarchically. When processing a query spectrum, the framework matches detected absorption peaks with graph entries and links them to corresponding "Range" nodes if spectral ranges align.

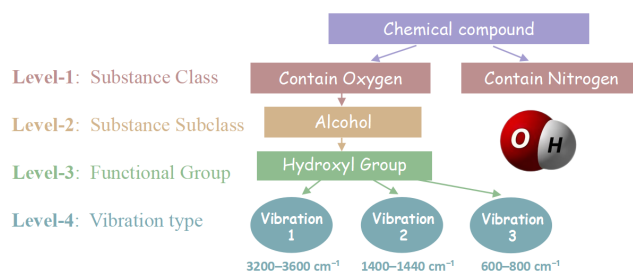


Figure 6: An example of TAG representation for chemical knowledge graph.

4.3. Dataset

We constructed a comprehensive dataset of 306 organic molecules, each annotated with infrared (IR) spectra and chemical properties, integrating structural and vibrational knowledge. This unified resource links molecular structure, functional group behavior, and spectral features, supporting tasks such as spectrum interpretation, molecular classification, and property prediction.

- **Spectral Data:** Sourced from SpectraPlot [37], which simulates high-precision IR spectra using databases like NIST ASD, HITRAN2012, and HITEMP2010. Each molecule's spectrum includes standardized absorption wavenumber and intensity data.
- **Chemical Knowledge Graph:** Built from an open-source framework [38], the graph includes hierarchical annotations-chemical family (e.g., alcohols, ketones), structural subclass (e.g., bonding patterns), and functional groups, which are key to chemical reactivity and spectral features.
- **Functional Group Information:** Extracted from Principles of Instrumental Analysis [39], this includes vibrational modes (e.g., stretching, bending), characteristic absorption wavenumbers, and absorbance intensities.

5. Experiments And Analysis

5.1. Experimental Settings and Baseline

All experiments in this chapter were conducted on a single NVIDIA 4090 GPU with 24GB of memory. Compared to models such as the H100 or A100, this setup is a significantly more cost-effective option, making it suitable for most research institutions and enterprises seeking to incorporate the advanced capabilities of LLMs into practical applications. For each model combination, the reported results represent the average classification performance and standard deviation obtained from ten independent inference runs under identical training and inference configurations. This approach helps to minimize the impact of random initialization and other potential sources of noise on the experimental outcomes.

In our experiments, we selected five commonly used open-source LLMs for encoding. Even though some models have relatively small parameter sizes (e.g., BERT), they are still considered important components of the LLMs family due to their pioneering role in ushering in the era of LLMs. The selected models include: (1) BERT [40], with a vector dimension of 1×768 and 110M parameters; (2) Sentence Transformer (ST) [41], with a vector dimension of 1×768 and 70M parameters; (3) e5 [42], with a vector dimension of 1×1024 and 330M parameters; (4) LLaMa2-7b [43], with a vector dimension of 1×4096 and 7 billion parameters; and (5) Qwen2-0.5b [44], with a vector dimension of 1×4096 and 550M parameters.

As a baseline for comparison, we also included the traditional Bag-of-Words (BoW) encoding method [45]. On

Table 1

Training Configuration of the Spectral Information Processing Framework across Different Downstream Tasks.

	Learning Rate	Dropout	Batch Size	Epoch
Node Classification	1e-3	0.005	32	10
Edge Classification	1e-5	0.005	1	5
Graph Judgement	1e-5	0.005	1	50
Graph Classification	1e-5	0.005	1	50

the other hand, we evaluated a range of classical GNN architectures: Graph Convolutional Networks (GCN) [46], Graph Attention Networks (GAT) [47], Graph Isomorphism Networks (GIN) [48], and Relational Graph Convolutional Networks (R-GCN) [49], to explore their performance when combined with different LLMs and identify the most effective pairing for optimal classification accuracy within our framework. For convenience, we still refer to this enhanced network structure as R-GCN.

5.2. Classification Tasks for Different Levels of Graphical Domains

We evaluated the LLM-based spectral information processing framework on four tasks: node classification, edge classification, graph identification, and graph classification. Training configurations are listed in Table 1, and results are summarized in Table 2. Accuracy (Acc) was used for multi-class node classification, while AUC ($\times 100$) was used for binary edge and graph tasks.

BoW encoding, lacking semantic understanding, performed poorly on binary tasks-failing to distinguish between semantically opposite inputs like "is" vs. "is not," resulting in an AUC of 0.5 due to uniform predictions. However, BoW performed moderately on multi-class tasks, achieving up to 62.14% accuracy for node classification and 98.12% for graph classification (both with R-GCN). Even so, these results were consistently outperformed by LLM-based encodings, with LLaMa2-7b+R-GCN reaching 67.64% accuracy on node classification and ST+GAT achieving 99.16% on graph classification.

LLM encodings significantly improved binary classification, with AUC scores nearing 100. However, node classification performance remained moderate. We attribute this to spectral ambiguity-overlapping absorption ranges among different functional groups-which limits the discriminative power of local information from single peaks. Since each "Prompt Node" links to only one "Absorption Node," the GNN's receptive field remains narrow. In traditional analysis, such ambiguity is resolved with multiple peaks or complementary spectra (e.g., Raman or MS), highlighting a current limitation of the framework under single-peak conditions. The baseline BoW encoder underperformed in binary tasks, achieving only 0.5 AUC due to its inability to capture semantics (e.g., distinguishing "is" vs. "is not"). However, it achieved moderate performance in multi-class tasks, with best results at 62.14% for node and 98.12% for graph classification using R-GCN-still lower than LLM-based encoders (e.g., LLaMa2-7b+R-GCN: 67.64% / 99.16%).

Table 2

Performance Evaluation of Different LLM Encoder and GNN Combinations in Different Downstream Tasks

Task Type Downstream Tasks	Node-Level	Edge-Level	Graph-Level	
	Node Classification (Acc)	Edge Classification (AUC×100)	Graph Judgement (AUC×100)	Graph Classification (AUC×100)
BoW+GCN	59.91 ± 0.79	Failed	Failed	98.49 ± 0.09
BoW+GAT	58.92 ± 0.59	Failed	Failed	97.45 ± 0.07
BoW+R-GCN	62.14 ± 0.94	Failed	Failed	98.12 ± 0.04
BoW+GIN	58.46 ± 2.20	Failed	Failed	88.85 ± 0.63
ST+GCN	60 ± 1.16	99.23 ± 0.01	98.7 ± 0.04	98.49 ± 0.09
BERT+GCN	54.26 ± 3.67	99.22 ± 0.04	98.39 ± 0.07	98.45 ± 0.14
e5+GCN	59.56 ± 1.49	99.22 ± 0.02	98.06 ± 0.16	98.47 ± 0.05
LLaMa2-7b+GCN	58.56 ± 0.17	99.83 ± 0.02	98.83 ± 0.29	98.46 ± 0.21
Qwen2-0.5b+GCN	58.1 ± 2.05	99.69 ± 0.05	97.01 ± 0.61	98.77 ± 0.19
ST+GAT	54.52 ± 6.73	99.21 ± 0.09	98.38 ± 0.64	99.16 ± 0.05
BERT+GAT	61.97 ± 1.00	97.69 ± 0.34	96.42 ± 0.58	97.22 ± 0.91
e5+GAT	53.12 ± 3.82	98.71 ± 0.21	98.09 ± 0.30	98.09 ± 0.41
LLaMa2-7b+GAT	50.64 ± 0.01	99.86 ± 0.01	98.26 ± 0.19	98.34 ± 0.10
Qwen2-0.5b+GAT	58.68 ± 0.41	98.18 ± 0.17	94.00 ± 4.62	95.01 ± 1.96
ST+R-GCN	63.04 ± 2.91	99.07 ± 0.04	98.84 ± 0.08	98.83 ± 0.12
BERT+R-GCN	63.98 ± 1.25	97.31 ± 0.04	98.55 ± 0.14	98.46 ± 0.08
e5+R-GCN	64.13 ± 2.89	98.68 ± 0.14	98.39 ± 0.09	98.30 ± 0.09
LLaMa2-7b+R-GCN	67.64 ± 0.02	99.71 ± 0.04	98.34 ± 0.00	98.67 ± 0.13
Qwen2-0.5b+R-GCN	56.67 ± 0.99	98.02 ± 0.06	91.83 ± 3.24	97.44 ± 0.59
ST+GIN	57.33 ± 1.47	99.41 ± 0.18	72.41 ± 7.36	84.98 ± 7.55
BERT+GIN	53.05 ± 10.47	99.54 ± 0.02	89.14 ± 2.43	78.14 ± 3.80
e5+GIN	45.59 ± 3.67	99.85 ± 0.11	66.02 ± 6.54	78.11 ± 3.69
LLaMa2-7b+GIN	56.67 ± 1.88	99.86 ± 0.03	68.78 ± 13.55	72.60 ± 4.33
Qwen2-0.5b+GIN	55.17 ± 3.26	99.86 ± 0.13	66.26 ± 9.54	77.73 ± 7.15

Regarding LLM encoding performance, LLaMa2-7b+R-GCN achieved the highest accuracy in node classification. For edge classification, LLaMa2-7b+GAT, LLaMa2-7b+GIN, and Qwen-0.5b+GIN all reached top AUC scores (99.86). In graph-level tasks, ST+R-GCN and ST+GAT delivered the best results. Notably, LLaMa2-7b consistently appeared in the best-performing combinations, suggesting it is the most effective encoder in this framework.

To assess overall performance across tasks, we fixed the GNN as R-GCN and aggregated scores (Accuracy + AUC*100) for each LLM:

- LLaMa2-7b+R-GCN: 364.36
- ST+R-GCN: 359.78
- BERT+R-GCN: 358.30
- e5+R-GCN: 359.50
- Qwen+R-GCN: 343.96

Despite differing metrics (Acc vs. AUC), all are scaled to a max of 100, making summation a reasonable approximation. These results confirm LLaMa2-7b as the most robust encoder overall.

For GNN comparison, we fixed LLaMa2-7b as the encoder and evaluated different architectures:

- LLaMa2+R-GCN: 364.36

- LLaMa2+GCN: 355.68
- LLaMa2+GAT: 347.10
- LLaMa2+GIN: 297.91

R-GCN outperformed other GNNs, likely due to its ability to model relational edges and apply attention mechanisms, yielding richer graph representations and more consistent results across tasks.

5.3. Zero-shot and Few-shot Capabilities

To assess in-context learning (ICL) abilities, we designed zero-shot and few-shot classification tasks using LLM-based embeddings in task graphs-critical for scenarios lacking labeled data. Inspired by traditional ICL paradigms, we introduced labeled reference samples as sub-graphs linked to target nodes (Figure 2). Each reference includes spectral connections and a "response node" with explicit class probabilities (true label = 100%).

To ensure a true zero-shot setting, we strictly isolated training and testing labels ($Y_{train} \cap Y_{test} = \emptyset$), requiring the model to classify unseen functional groups using only reference samples and prior knowledge.

We evaluated four classification tasks using two LLM-GNN configurations: ST+R-GCN and BERT+R-GCN. The GNN was fixed to R-GCN for consistency, while ST and BERT were selected as moderate baselines. Tasks were

Table 3

Performance of Different Model Combinations in ICL Capability Across Various Downstream Tasks

Task Type	Node-Level		Edge-Level		Graph-Level			
Downstream Tasks	Node Classification (Acc)		Edge Classification (AUC*100)		Graph Judgement (AUC*100)		Graph Classification (AUC*100)	
	BERT	ST	BERT	ST	BERT	ST	BERT	ST
0-shot	39.74 ± 1.13	39.8 ± 0.68	59.07 ± 6.65	73.07 ± 1.16	23.33 ± 3.73	47.5 ± 5.59	20.83 ± 4.17	40 ± 5.59
1-shot	43.74 ± 8.07	20.83 ± 6.72	72.23 ± 7.1	81.3 ± 5.78	55.47 ± 12.92	73.34 ± 6.09	43.57 ± 8.6	66.67 ± 13.61
3-shots	43.97 ± 7.46	26.19 ± 4.45	80.3 ± 2.08	86.89 ± 0.85	56.19 ± 15.21	75 ± 8.33	53.37 ± 7.82	70 ± 15.14
5-shots	47.93 ± 7.09	27.83 ± 4.95	83.92 ± 1.59	88.27 ± 1.81	63.33 ± 9.5	68.75 ± 6.25	72.5 ± 8.64	72.08 ± 4.06

Table 4

Training Configuration of the Spectral Information Processing Framework for ICL Capability

	Learning Rate	Dropout	Batch Size	Epoch
Node Classification	1e-3	0.05	1	50
Edge Classification	1e-5	0.05	1	50
Graph Judgement	1e-5	0.05	1	50
Graph Classification	1e-5	0.05	1	50

tested under 0-shot, 1-shot, 3-shot, and 5-shot settings (configurations in Table 4, results in Table 3).

In the zero-shot edge classification task, both models exceeded AUC 50, indicating basic ICL capability. However, performance in node and graph-level tasks remained below threshold, suggesting that the LLMs' limited parameter size and the GNN's coarse aggregation hinder deeper semantic reasoning. Notably, the framework struggled to follow prompts precisely in these tasks.

In few-shot settings, performance generally improved with more reference examples, especially in edge and graph classification. However, node classification remained unstable. For example, ST achieved its best node-level accuracy in 0-shot, while BERT peaked at 5-shot. Similarly, in graph judgment, ST's best result occurred at 3-shot (75 ± 8.33), not 5-shot.

Overall, the framework shows the initial ICL capability—especially in edge-level zero-shot tasks—and benefits from few-shot enhancement. However, instability across tasks and weak node-level performance highlight current limitations, primarily due to the modest capacity of selected LLMs and GNNs' inability to fully leverage semantic embeddings. Future work should explore more powerful LLMs and refined graph integration strategies to enhance ICL performance.

5.4. Framework Optimization Analysis

This section analyzes key module configurations within the framework and their impact on classification performance, focusing on prompt formats and training strategies. All experiments use the R-GCN+BERT configuration.

5.4.1. Simple Prompts vs. Detailed Prompts

The "Prompt Node" serves as a critical interface for conveying task intent, and its textual format can significantly affect model performance. To evaluate this, we compared two prompt styles (Figure 7):

- **Detailed Prompts:** Multi-sentence natural language descriptions (~6–7 sentences), offering rich task context.
- **Simple Prompts:** Brief labels (e.g., "Task1") with one short sentence indicating the expected output.

Simple Prompt

Prompt node. node classification on the sample's category based on the spectral information and the knowledge graph.

Detailed Prompt

Prompt node. Based on the knowledge graph and spectral data, classify the functional group of the molecular node. Use the knowledge graph to identify functional group associations and validate the classification decision with relevant spectral evidence. Classify the molecule into categories based on the detected functional group and provide justification using spectral peak information and knowledge graph relationships.

Figure 7: An example comparing a simple prompt with a detailed prompt.

Results (Table 5) show that Detailed Prompts outperformed in edge and graph tasks, yielding higher AUC scores (98.79 ± 0.01 , 98.57 ± 0.05 , and 98.49 ± 0.11). However, in node-level classification, Simple Prompts slightly outperformed (66.43 ± 0.17 vs. 64.57 ± 0.08). This is likely due to limited receptive fields in node tasks, where overly detailed prompts may introduce noise, while concise prompts maintain clarity. In contrast, multi-node connections in edge and graph tasks benefit from detailed context, enabling better information propagation and discrimination.

In summary, Detailed Prompts are generally preferable, especially for edge and graph-level tasks, as they improve task comprehension and align more closely with natural, interpretable communication.

5.4.2. Single-Task Training vs. Multi-Task Training

While training separate GNNs for each task is intuitive, it is often impractical in real-world scenarios due to the difficulty of collecting large-scale data for a single task. In contrast, assembling smaller datasets across multiple tasks is more feasible. Given the framework's unified task graph structure, Multi-Task training can be naturally implemented. This experiment compares the two strategies

Table 5

Classification Performance under Different Prompt Description in the Spectral Information Processing Framework

Task Type	Node-Level	Edge-Level	Graph-Level	
Downstream Tasks	Node Classification (Acc)	Edge Classification (AUC)	Graph Judgement (AUC)	Graph Classification (AUC)
Simple Prompts	66.43 \pm 0.17	96.78 \pm 0.18	98.45 \pm 0.08	98.46 \pm 0.08
Detailed Prompts	64.57 \pm 0.08	98.79 \pm 0.01	98.57 \pm 0.05	98.49 \pm 0.11

Table 6

Experimental Results of Single-Task Training and Multi-Tasks Training

Task Type	Node-Level	Edge-Level	Graph-Level	
Downstream Tasks	Node Classification (Acc)	Edge Classification (AUC*100)	Graph Judgement (AUC*100)	Graph Classification (AUC*100)
Single-Task Training	61.97 \pm 1	97.69 \pm 0.34	96.42 \pm 0.58	97.22 \pm 0.91
Multi-Tasks Training	60.07 \pm 1.02	97.78 \pm 0.12	97.43 \pm 0.22	98.09 \pm 0.43

to assess whether Multi-Task training can match or surpass Single-Task performance.

Unlike the ICL setting in Section 5.3, where model parameters remain unchanged, Multi-Task training involves joint parameter optimization. Here, a mixed dataset (with one-third samples from each task type) is compared against standard single-task datasets (4n samples per task). Results are shown in Table 6.

In node classification, Multi-Task training slightly underperforms (60.07 \pm 1.02 vs. 61.97 \pm 1.00), likely due to task interference. However, it outperforms Single-Task training in edge and graph-level tasks. This indicates the framework can distinguish different task prompts during joint training, thanks to the semantic expressiveness of LLM-based embeddings.

Overall, Multi-Task training achieves comparable results with added benefits in scalability and data efficiency, making it a practical alternative. Future work will explore strategies to mitigate inter-task conflicts, especially to improve node-level performance.

5.5. Spectrum Simulation

Given a query like "What is the spectrum of cyclohexanone?", a fine-tuned LLM (Qwen2.5-Math-1.5B-Instruct via LoRA [50]) first extracts the chemical formula. We trained the models on 1600 molecular samples and evaluated them on a separate set of 200 molecules. Performance was assessed using BERT-Score and ROUGE to measure the accuracy of chemical formula extraction and molecular structure prediction. Results are shown in Tables 7 and 8.

LLM 1 achieved perfect scores across all metrics (Rouge-1, Rouge-L, precision, recall, F1 = 100), demonstrating

excellent performance on well-defined inputs aligned with training data. LLM 2 performed slightly lower (Rouge-1: 61.59, Rouge-2: 30.09, Rouge-L: 49.11) but still maintained high precision and F1 score (94.99), indicating reliable performance on more complex or ambiguous inputs. These results confirm the effectiveness of the generation task of the model and highlight the value of integrating external knowledge bases to enhance molecular data processing.

Spectral simulation performance was assessed using R^2 , RMSE, and MAE. For NIR spectra, the model achieved an R^2 of 93.99, with very low RMSE (3.89e-5) and MAE (8.41e-6), indicating high prediction accuracy. For Raman spectra, R^2 was also 93.99, with higher RMSE (0.135) and MAE (0.026), still demonstrating robust performance given the complexity of the data. UV spectrum simulation yielded an R^2 of 94.99, with low RMSE (0.0016) and MAE (0.006), confirming strong predictive ability.

These results demonstrate that fine-tuned LLMs can accurately simulate NIR, Raman, and UV spectra directly from chemical formulas, marking a significant advancement in language-driven spectral data generation and model efficiency.

5.6. Conclusion

In this study, we proposed a spectral information processing framework based on LLMs embeddings, which utilizes TAG as a unified representation for multi-modal data. This framework maps the textual information from the graph into a shared semantic space using LLMs. The text-based graph representation serves as a medium for interaction among heterogeneous data modalities and incorporates both the prior knowledge and ICL capabilities acquired by LLMs

Table 7

Evaluation result of finetuned LLMs

Metrics	Rouge Scores			Bert Scores		
	Rouge-1	Rouge-2	Rouge-L	Precision	Recall	F1 Score
LLM for extracting molecular formula	100	93	100	100	100	100
LLM for generating tensors	61.59	30.09	49.11	94.99	94.99	94.99

Table 8

Test result of spectrum simulation

Metrics	R2	RMSE	MAE
NIR spectrum simulation	93.99	3.89e-5	8.41e-6
Raman spectrum simulation	93.99	0.135	0.026
UV spectrum simulation	94.99	0.0016	0.006

through large-scale pretraining. By jointly encoding physical spectral signals and chemically structured knowledge, the framework enables cross-modal reasoning grounded in both measurement and molecular semantics. We further elaborated on the transformation of various data types—such as spectral data, textual literature, and knowledge graphs—into this unified graph format. Additionally, we introduced the task sub-graph structure, which enables users to flexibly define and switch among different downstream tasks via natural language prompts. This design allows for the integration of node-level, edge-level, and graph-level tasks within a single, coherent framework. To evaluate the framework’s effectiveness, we conducted experiments on a mid-infrared molecular spectroscopy dataset, assessing performance across multiple tasks and examining its ICL potential. Experimental results show that the framework achieves near-perfect AUC scores on both edge-level and graph-level tasks and demonstrates initial ICL capabilities. These findings strongly support the framework’s applicability in practical, application-oriented spectral analysis scenarios.

CRedit authorship contribution statement

Jiheng Liang: Methodology, Data curation, Validation, Formal analysis, Visualization, Writing – original draft. **Ziru Yu:** Conceptualization, Methodology, Validation, Visualization, Writing – original draft, Writing – review & editing, Project administration. **Zujie Xie:** Data curation, Validation, Formal analysis, Software, Writing – original draft. **Yuchen Guo:** Investigation, Validation, Formal analysis, Software. **Yulan Guo:** Supervision, Funding acquisition, Project administration. **Xiangyang Yu:** Supervision, Resources, Writing – review & editing.

Declaration of Competing Interest

The authors declare that they have no known competing financial interests or personal relationships that could have appeared to influence the work reported in this paper.

Code and Data Availability

The code will be made publicly available upon acceptance. The datasets are available from the corresponding author upon reasonable request.

References

[1] J. Workman Jr, Exploring the spectrum of analytical techniques for material characterization (2023).

[2] R. S. Das, Y. Agrawal, Raman spectroscopy: Recent advancements, techniques and applications, *Vibrational spectroscopy* 57 (2) (2011) 163–176.

[3] S. Maithani, M. Pradhan, Cavity ring-down spectroscopy and its applications to environmental, chemical and biomedical systems, *Journal of Chemical Sciences* 132 (2020) 1–19.

[4] S. Weiss, Fluorescence spectroscopy of single biomolecules, *Science* 283 (5408) (1999) 1676–1683.

[5] Y. Li, J.-Y. Zhang, Y.-Z. Wang, Ft-mir and nir spectral data fusion: A synergetic strategy for the geographical traceability of panax notoginseng, *Analytical and bioanalytical chemistry* 410 (2018) 91–103.

[6] D. Lahat, T. Adali, C. Jutten, Multimodal data fusion: An overview of methods, challenges, and prospects, *Proceedings of the IEEE* 103 (9) (2015) 1449–1477. doi:10.1109/JPROC.2015.2460697.

[7] J. Gao, P. Li, Z. Chen, J. Zhang, A survey on deep learning for multimodal data fusion, *Neural Computation* 32 (5) (2020) 829–864. arXiv:https://direct.mit.edu/neco/article-pdf/32/5/829/1865303/neco_a_01273.pdf, doi:10.1162/neco_a_01273. URL https://doi.org/10.1162/neco_a_01273

[8] M. Pawłowski, A. Wróblewska, S. Sysko-Romańczuk, Effective techniques for multimodal data fusion: A comparative analysis, *Sensors* 23 (5) (2023). doi:10.3390/s23052381. URL https://www.mdpi.com/1424-8220/23/5/2381

[9] E. R. Neo, J. S. Low, V. Goodship, S. R. Coles, K. Debattista, Cross-modal generative models for multi-modal plastic sorting, *Journal of Cleaner Production* 415 (2023) 137919.

[10] T. Xing, Y. Dou, X. Chen, J. Zhou, X. Xie, S. Peng, An adaptive multi-graph neural network with multimodal feature fusion learning for mdd detection, *Scientific Reports* 14 (1) (2024) 28400.

[11] Y. Zhu, L. F. Tadesse, Universal spectral transfer with physical prior-informed deep generative learning, arXiv preprint arXiv:2407.16094 (2024).

[12] J. Achiam, S. Adler, S. Agarwal, L. Ahmad, I. Akkaya, F. L. Aleman, D. Almeida, J. Altenschmidt, S. Altman, S. Anadkat, et al., Gpt-4 technical report, arXiv preprint arXiv:2303.08774 (2023).

[13] M. V. Koroteev, Bert: a review of applications in natural language processing and understanding, arXiv preprint arXiv:2103.11943 (2021).

[14] C. Zhou, Q. Li, C. Li, J. Yu, Y. Liu, G. Wang, K. Zhang, C. Ji, Q. Yan, L. He, et al., A comprehensive survey on pretrained foundation models: A history from bert to chatgpt, *International Journal of Machine Learning and Cybernetics* (2024) 1–65.

[15] P. Kaur, G. S. Kashyap, A. Kumar, M. T. Nafis, S. Kumar, V. Shokeen, From text to transformation: A comprehensive review of large language models’ versatility, arXiv preprint arXiv:2402.16142 (2024).

[16] H. Gani, S. F. Bhat, M. Naseer, S. Khan, P. Wonka, Llm blueprint: Enabling text-to-image generation with complex and detailed prompts, arXiv preprint arXiv:2310.10640 (2023).

[17] J. Wei, J. Wei, Y. Tay, D. Tran, A. Webson, Y. Lu, X. Chen, H. Liu, D. Huang, D. Zhou, et al., Larger language models do in-context learning differently, arXiv preprint arXiv:2303.03846 (2023).

[18] J. Summaira, X. Li, A. M. Shoib, S. Li, J. Abdul, Recent advances and trends in multimodal deep learning: A review, arXiv preprint arXiv:2105.11087 (2021).

[19] W. Guo, J. Wang, S. Wang, Deep multimodal representation learning: A survey, *Ieee Access* 7 (2019) 63373–63394.

[20] T. Zhou, M. Liu, K.-H. Thung, D. Shen, Latent representation learning for alzheimer’s disease diagnosis with incomplete multi-modality neuroimaging and genetic data, *IEEE transactions on medical imaging* 38 (10) (2019) 2411–2422.

[21] K. Mao, W. Zhang, D. B. Wang, A. Li, R. Jiao, Y. Zhu, B. Wu, T. Zheng, L. Qian, W. Lyu, et al., Prediction of depression severity based on the prosodic and semantic features with bidirectional lstm and time distributed cnn, *IEEE transactions on affective computing* 14 (3) (2022) 2251–2265.

[22] F. Agbavor, H. Liang, Artificial intelligence-enabled end-to-end detection and assessment of alzheimer’s disease using voice, *Brain sciences* 13 (1) (2022) 28.

- [23] S. Zhou, N. Wang, L. Wang, H. Liu, R. Zhang, Cancerbert: a cancer domain-specific language model for extracting breast cancer phenotypes from electronic health records, *Journal of the American Medical Informatics Association* 29 (7) (2022) 1208–1216.
- [24] X. Li, S. Sun, T. Tang, J. Lu, L. Zhang, J. Yin, Q. Geng, Y. Wu, Construction of a knowledge graph for breast cancer diagnosis based on chinese electronic medical records: development and usability study, *BMC Medical Informatics and Decision Making* 23 (1) (2023) 210.
- [25] R. Wang, A multi-modal knowledge graph platform based on medical data lake, in: *International Conference on Web Information Systems and Applications*, Springer, 2022, pp. 15–27.
- [26] H. Yu, Y. Li, W. Du, M. Yang, X. Peng, X. Wang, J. Long, A novel interpretable ensemble learning method for nir-based rapid characterization of petroleum products, *IEEE Transactions on Instrumentation and Measurement* (2023).
- [27] T. Tu, S. Azizi, D. Driess, M. Schaeckermann, M. Amin, P.-C. Chang, A. Carroll, C. Lau, R. Tanno, I. Ktena, et al., Towards generalist biomedical ai, *NEJM AI* 1 (3) (2024) A10a2300138.
- [28] Y. Yang, S. Sun, M. Huang, Q. Zhu, Peamatl: A strategy for developing near-infrared spectral prediction models under domain shift using self-supervised transfer learning, *IEEE Transactions on Instrumentation and Measurement* 72 (2023) 1–12.
- [29] J. Zhou, P. Ke, X. Qiu, M. Huang, J. Zhang, Chatgpt: potential, prospects, and limitations, *Frontiers of Information Technology & Electronic Engineering* (2023) 1–6.
- [30] M. Rele, A. Julian, D. Patil, U. Krishnan, Multimodal data fusion integrating text and medical imaging data in electronic health records, in: *International Conference on Innovations and Advances in Cognitive Systems*, Springer, 2024, pp. 348–360.
- [31] H. Liu, J. Feng, L. Kong, N. Liang, D. Tao, Y. Chen, M. Zhang, One for all: Towards training one graph model for all classification tasks, *arXiv preprint arXiv:2310.00149* (2023).
- [32] Z. Zou, Y. Zhang, L. Liang, et al., A deep learning model for predicting selected organic molecular spectra, *Nature Computational Science* 3 (2023) 957–964. doi:10.1038/s43588-023-00550-y. URL <https://doi.org/10.1038/s43588-023-00550-y>
- [33] J. Liang, Z. Yu, Z. Xie, X. Yu, A quick, trustworthy spectral knowledge q&a system leveraging retrieval-augmented generation on llm, *arXiv preprint arXiv:2408.11557* (2024).
- [34] M. Delmas, O. Filangi, N. Paulhe, F. Vinson, C. Duperier, W. Garrier, P.-E. Saunier, Y. Pitarch, F. Jourdan, F. Giacomoni, et al., building a knowledge graph from public databases and scientific literature to extract associations between chemicals and diseases, *Bioinformatics* 37 (21) (2021) 3896–3904.
- [35] X. Lin, Z. Quan, Z.-J. Wang, T. Ma, X. Zeng, Kgnn: Knowledge graph neural network for drug-drug interaction prediction., in: *IJCAI*, Vol. 380, 2020, pp. 2739–2745.
- [36] Y. Fang, Q. Zhang, N. Zhang, Z. Chen, X. Zhuang, X. Shao, X. Fan, H. Chen, Knowledge graph-enhanced molecular contrastive learning with functional prompt, *Nature Machine Intelligence* 5 (5) (2023) 542–553.
- [37] SpectraPlot, Wavelength references, spectraPlot: A web-based spectral simulation tool for molecular absorption analysis (n.d.). URL <https://www.spectraplot.com>
- [38] Y. Fang, Q. Zhang, N. Zhang, et al., Knowledge graph-enhanced molecular contrastive learning with functional prompt, *Nature Machine Intelligence* 5 (2023) 542–553. doi:10.1038/s42256-023-00654-0. URL <https://doi.org/10.1038/s42256-023-00654-0>
- [39] D. A. Skoog, F. J. Holler, S. R. Crouch, *Principles of Instrumental Analysis*, 7th Edition, Cengage Learning, 2007.
- [40] J. Devlin, M.-W. Chang, K. Lee, K. Toutanova, Bert: Pre-training of deep bidirectional transformers for language understanding (2019) 4171–4186.
- [41] N. Reimers, I. Gurevych, Sentence-bert: Sentence embeddings using siamese bert-networks, *arXiv preprint arXiv:1908.10084* (2019).
- [42] L. Wang, N. Yang, X. Huang, B. Jiao, L. Yang, D. Jiang, R. Majumder, F. Wei, Text embeddings by weakly-supervised contrastive pre-training, *arXiv preprint arXiv:2212.03533* (2022).
- [43] H. Touvron, T. Lavril, G. Izacard, X. Martinet, M.-A. Lachaux, T. Lacroix, B. Rozière, N. Goyal, E. Hambro, F. Azhar, et al., Llama: Open and efficient foundation language models, *arXiv preprint arXiv:2302.13971* (2023).
- [44] A. Yang, B. Yang, B. Zhang, B. Hui, B. Zheng, B. Yu, C. Li, D. Liu, F. Huang, H. Wei, et al., Qwen2. 5 technical report, *arXiv preprint arXiv:2412.15115* (2024).
- [45] Y. Zhang, R. Jin, Z.-H. Zhou, Understanding bag-of-words model: a statistical framework, *International journal of machine learning and cybernetics* 1 (2010) 43–52.
- [46] T. N. Kipf, M. Welling, Semi-supervised classification with graph convolutional networks, *arXiv preprint arXiv:1609.02907* (2016).
- [47] P. Veličković, G. Cucurull, A. Casanova, A. Romero, P. Lio, Y. Bengio, Graph attention networks, *arXiv preprint arXiv:1710.10903* (2017).
- [48] K. Xu, W. Hu, J. Leskovec, S. Jegelka, How powerful are graph neural networks?, *arXiv preprint arXiv:1810.00826* (2018).
- [49] M. Schlichtkrull, T. N. Kipf, P. Bloem, R. Van Den Berg, I. Titov, M. Welling, Modeling relational data with graph convolutional networks, in: *The semantic web: 15th international conference, ESWC 2018, Heraklion, Crete, Greece, June 3–7, 2018, proceedings* 15, Springer, 2018, pp. 593–607.
- [50] E. J. Hu, Y. Shen, P. Wallis, Z. Allen-Zhu, Y. Li, S. Wang, L. Wang, W. Chen, Lora: Low-rank adaptation of large language models, *arXiv preprint arXiv:2106.09685* (2021). URL <https://arxiv.org/abs/2106.09685>